International Journal of Technology

http://ijtech.eng.ui.ac.id

Type of the Paper (Research Article)

Numerical Study the stability of STU.1.M Drone at the Unsteady State Conditions

Sabah Sameer Abood Almukhtar [1*], Mohammed A. Abdulwahid[2], Akeel MA Morad [3,]

[1]*Department of Thermal Mechanics Engineerin Technical Engineering College/Basra, Southern technical university, Basra, Iraq;*
[2] *Department of Thermal Mechanics Engineerin Technical Engineering College/Basra, Southern technical university, Basra, Iraq;*
[3]*Department of Thermal Mechanics Engineerin Technical Engineering College/Basra, Southern technical university, Basra, Iraq;*

[*]Corresponding author: Sabah.s.almukhtar@fgs.stu.edu.iq; Tel.: +964 782 793 2232;

Abstract: Unmanned aerial vehicles, or UAVs, are becoming more and more important in a variety of industries, including agriculture, civil aviation, the military, and the environment.: In this study, we investigated the aerodynamic stability of a transient STU.1.M unmanned aerial vehicle (UAV) At speeds of 40, 60, and 80 m/s and an angle of attack of 6 degrees, corresponding to the lift-to-drag coefficient ratio's maximum value in a steady state. For the numerical analysis, Ansys Fluent was used. The grid-independence study and validity of the numerical solution were conducted by comparing the results of the proposed mathematical model on NACA 0012 airfoil with experimental results using same mathematical model. The numerical study revealed that vortices formed and decay behind the aircraft as a result of the flow field's oscillations at specific frequencies. The magnitude of these vortices grows as the aircraft's speed increases. When the aircraft speed is increased to 80 m/s, the lift coefficient increases by 0.56%, while the lift-to-drag ratio increases by 2.85%. The lift-to-drag ratio oscillation frequency rises by 102.5%, while the vertical oscillation frequency, which corresponds to the oscillations of the lift force, decreased by 71.7%.

Keywords: Drag; Lift; CFD; UAV; Frequency.

For grants, please provide the grant number and the year it was received. Write it as follows: "This work was supported by the 'Name of organization' funded by 'Name of Grant and number' "

https://doi.org/xx/ijtech.xx
Received date; Revised date; Accepted date

1. Introduction

Unmanned Aerial Vehicles, or UAVs for short, are autonomous aircraft that operate without a human pilot operating the flight controls (Dickes et al. 2000). Because UAVs have the potential to benefit the aircraft industry, they are being closely examined and are continuously evolving. Benefits include being less costly than conventional jet aircraft, not endangering pilots, being able to fly autonomously for longer periods of time than a human pilot, and being able to fly in regions that are considered too hazardous for pilots to fly in (Boelens 2012). The motion and interaction of air around and with solid objects are of interest in the subfield of fluid dynamics known as aerodynamics. When objects move in the air at limited speeds so that the Mach number of the flow does not exceed 0.3, as is the case when flying drones, then the density changes are small and the flow is then called incompressible fluid flow and the changes in forces and momentum are then linear and this science is called linear aerodynamics (Klein & Morelli 2006). In contemporary engineering, time-varying fluid flows and their unsteady aerodynamic forces and moments are commonplace. Cars, boats, and airplanes are all designed with meticulous optimization to streamline the body and increase efficiency by reducing drag and flow separation (Kubo 2006).

(Molaa & Abdulwahid 2024) conducted a numerical and experimental study of the impact effect on the aerodynamic properties of the NACA0012 airfoil, with the results showing remarkable agreement between the numerical modeling and practical tests, contributing to a better understanding of the airfoil performance under turbulent conditions. (Song, Zhao, & Liu 2023) comprehensively reviewed mission planning methods for UAV fleets, categorizing different strategies according to missions and operational environments, and highlighting technical challenges and future trends in this field. (Zhang et al. 2024) conducted an experimental and numerical study on the secondary flow systems of a supersonic aircraft wing, using a wind tunnel to simulate actual flight conditions, and the results showed good agreement between the numerical simulation and tests, which contributes to the improvement of supersonic wing design.

(Maleki Dastjerdi et al. 2021) presented an innovative design for vertical axis wind turbines using a simultaneous combination of symmetric and curved airfoils. The results showed improved aerodynamic performance compared to conventional designs, enhancing the potential of these turbines in diverse environments. (Majid & Jo 2021) conducted a comparative study between the aerodynamic performance of conventional and camber morphing airfoils, where camber morphing airfoils showed improved performance in terms of lift and aerodynamic efficiency, indicating their potential in advanced aviation applications. (Somashekar 2021) conducted a comparative study to evaluate the accuracy of different turbulence models in predicting the aerodynamic properties of small unmanned aerial vehicles. The results showed that the performance of the models varied in representing the airflow, which helps in choosing the most appropriate model to improve the simulation accuracy. (Mubassira et al. 2021) conducted a numerical study of the characteristics of the NACA 4312 airfoil when a Gurney slat was added. The results showed a significant improvement in lift force without a significant increase in drag force, indicating the effectiveness of the slat in improving the aerodynamic performance of airfoils.

The potential of unsteady aerodynamics for engineering design is perhaps best demonstrated by biological propulsion. It has been noted that fish, insects, birds, and bats frequently use unsteady fluid dynamics to enhance their maneuverability, maximize thrust and lift, and improve their propulsive efficiency (Roy et al. 2007). Unsteady aerodynamic forces are becoming more significant during agile maneuvers and gust disturbances as unmanned aerial vehicles (UAVs) get lighter and smaller. Over the past century, the need for precise, effective aerodynamic models has

served as a major driving force behind research efforts. In order to design aircraft and assess aeroelastic and flight dynamic stability, aerodynamic models are essential tools (Selig 2010).

The quasi-steady assumption that forces and moments depend statically on parameters like relative velocity and angle of attack is the foundation of the majority of aerodynamic models used for flight control. The unsteady aerodynamic forces necessary for small, agile aircraft to avoid obstacles, react to gusts, and track potentially elusive targets are not described by these models, despite the fact that they perform well for conventional aircraft (Schlichting & Truckenbrodt 1979; Leishman 2006). Nonetheless, the literature contains a large number of unsteady aerodynamic models. The classical unsteady models of Theodorsen (Theodorsen 1979; Wagner 2006) are still in use today and serve as a standard for the linear models that come after them. By convolving the motion's time derivative with the analytically calculated step response, Wagner's model generates the lift in response to arbitrary input motion. Theodorsen used the same model assumptions of an incompressible, inviscid, planar wake to create an analogous model in the frequency domain. With the resources available at the time, Theodorsen's model was appropriate for the analysis of flutter instability even though it only applies to sinusoidal input motion. Direct numerical simulations (DNS) (Williams et al. 2008; Taira & T. Colonius 2009), computational fluid dynamics (CFD) (Taira & T. I. M. Colonius 2009; Sitaraman & Baeder 2004; Murman 2007; Singh & Baeder 1997; Ronch et al. 2012; Amsallem et al. 2010), wind tunnel experiments (Pelletier & Mueller 2000; Williams et al. 2008), and water channel experiments (Fransos & Bruno 2006; Buchholz & Smits 2008) can all be used to create sophisticated models for the unsteady fluid dynamics and the resulting aerodynamic forces. The viscous fluid dynamic interactions that result in transient unsteady aerodynamics may be accurately estimated using any of these techniques. These techniques, however, are very costly in terms of both time and equipment. Therefore, it is crucial to extract low-dimensional models from these intricate model systems (Green & Smits 2008; Ol et al. 2005; Dowell et al. 1997; Gold & Karpel 2008; Mor & Livne 2005; Silva & Bartels 2004).

A model for small fixed-wing UAVs at high angles of attack is presented by (Johnson & Lind 2009) and is based solely on flight test data. Transfer functions from aileron, elevator, and rudder commands to roll, pitch, and yaw rates are found using least square regression curve fitting. For example, a controller for the hover maneuver of a small fixed-wing MAV is presented by (Green & Oh 2005; Green & Oh 2009). Since nonlinear or unsteady aerodynamics are not involved, the controller's dynamics are modeled using first principles and simplified. (Kaplan et al. 2007) Discuss the Reynolds number and aspect ratio on small wings. For larger amplitude maneuvers at high angles of attack, nonlinear separated flow effects like vortex shedding (Leishman et al. 2002) and dynamic stall (Fischenberg & Jategaonkar 1998) are crucial.

It is worth mentioning that novel materials, such as Polyethylene Terephthalate (PET) (Patel, 2023), present robust substances can address critical performance challenges to drone stability under unsteady conditions. Modern numerical studies must evaluate such trade-offs for the STU.1.M drone. Additionally, The STU.1.M drone's stability under turbulent conditions considers economic issues and climate change that disturb food and medical supply chains (Sharma, 2024). On this regard, this study's numerical investigation could help in designing drones for such high-stakes environments.

This research is a continuation of the study of the aerodynamic stability of the flow through the STU.1.M aircraft, in which the changes in the values of CL, CD and CL/CD were studied over the entire aircraft body with the change in the angle of attack in the steady state, and it was found that the optimum angle value for which the value of CL/CD is the maximum is the angle of 6 degrees. Therefore, this research aims to study the behavior and aerodynamic stability at this angle (6 degrees) in the unsteady state using numerical modeling at 40, 60, and 80 m/sec aircraft velocity in

order to evaluate the aerodynamic performance of the aircraft resulting from the fluctuation of the flow field as a result of its passage through the aircraft body.

2. Materials and Methods

Flow-induced vibration (FIV) is defined as the mechanical vibration of structures within a fluid flow or fluid carrier (such as pipes). Many engineering structures are subject to the interaction between aerodynamic forces, inertial forces, damping and elasticity of these structures (Bernitsas et al. 2008). This phenomenon is of particular importance in non-streamlined structures, which are more susceptible to this phenomenon due to their exposure to boundary layer separation. The aerodynamic forces that affect a body in a flow, regardless of its shape, are caused by two factors: the distribution of pressure and the shear stress resulting from viscosity on the immersed surface of the body. Pressure affects the body tangentially, causing lift, while shear stress affects the surface of the body tangentially, causing drag (Bibo & Daqaq 2015). Under certain conditions, these forces cause the body to move, which in turn changes the position of the body relative to the flow, causing a change in the aerodynamic forces and the occurrence of a vibration phenomenon resulting from the flow (Blevins, 1977).

The lift and drag coefficient values affecting the STU.1.M UAV were determined in this study using unsteady CFD numerical modeling, and the following relationships were identified (Blevins, 1977):

$$C_L = \frac{F_L}{0.5\rho V^2 A} \quad , C_D = \frac{F_D}{0.5\rho V^2 A} \qquad (1)$$

where A is the area of the UAV projection on a plane perpendicular to the flow direction (m^2), V is the UAV speed (m/sec), and FL and FD stand for lift and drag force (N), respectively, and ρ is air density (Kg/m^3) (Blevins, 1977) . The numerical solution was carried out using Ansys Fluent. SolidWorks was used to draw the UAV model and the surrounding fluid domain, and Ansys meshing was used to create the mesh. The mesh was then exported to Fluent for the numerical solution. A 3970 x 32 core AMD thread ripper computer with 128 GB of DDR5 RAM was utilized.

Drawing a model of the UAV in use and creating the fluid domain around it are the first stages of numerical modelling. SolidWorks' software was used to draw the aircraft model in its actual dimensions. A diagram of the drawn UAV is shown in Figure 1, and the drone's characteristic values are displayed in Table 1.

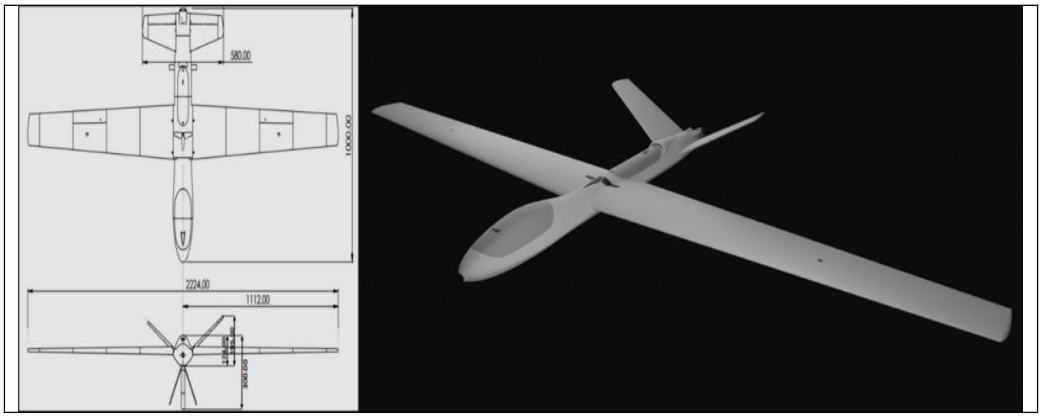

Figure 1 Main dimensions of studied UAV

Table 1 Designed parameters of studied UAV.

No.	Dimensions	The symbol	Value

1	Wing length	L	105 cm
2	Wing span	b	224 cm
3	Root chord	cr	29 cm
4	Tip chord	ct	12.4 cm
5	Aspect ratio	AR	12.9
6	Taper ratio	λ	0.42
7	Wing area	A	4636.8 cm^2
8	Dihedral	D	0
9	Sweep	s	0
10	Chord line	c	20.7cm

The wing used is a Taper type wing NACA 2410 and the tail is a V-type.

In order to minimize flow distortion, domain type C is utilized in this paper to minimize mesh and expedite the solution process. The plane location is five times the chord length upstream and ten times downstream. Four faces make up the domain; the wing side and inlet side have an area of 1.2397 m^2, the outlet side has an area of 102.02 m^2, and the inlet side has an area of 298.94 m^2. As seen in Figure 2, the bounding box (length x = 4.379 m, length y = 23.296 m, length z = 29.813 m).

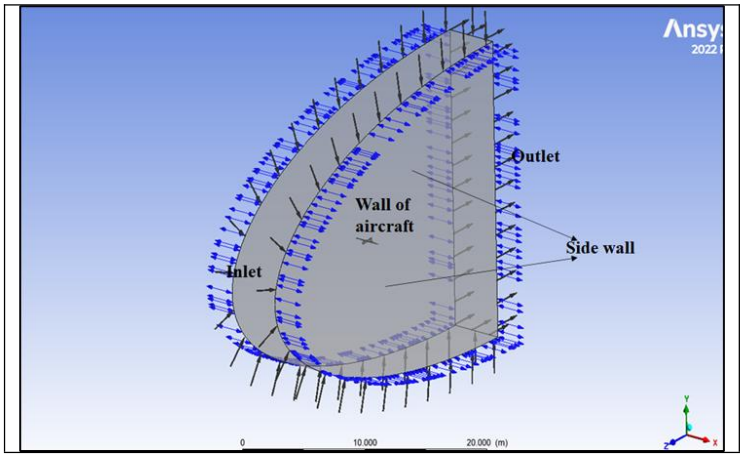

Figure 2 Fluid Domain and Boundary Conditions

2.1 Mathematical model

Computational fluid dynamics, or CFD for short, is a powerful tool used in modeling involving fluid flow. There is many commercial software that use this science to analyze engineering systems, solve them, and display the results. Solving this problem numerically involves solving a set of differential equations that describe this movement. These equations include the continuity equation and the momentum equations, which are given by the following relationships (Andersson et al. 2012):

$$\frac{\partial \rho}{\partial t} + \frac{\partial (\rho u)}{\partial x} + \frac{\partial (\rho v)}{\partial y} + \frac{\partial (\rho w)}{\partial z} = 0 \quad (2)$$

The continuity equation expresses the law of conservation of mass within the control volume under consideration and states that the net time rate of mass entering and leaving must equal the change in mass within the control volume with time.

where ρ is the Fluid density, u,v and w is the velocity components on the x, y and z direction. Momentum equations on X, Y and Z direction are (Chaoqun. L, Jiyuan. T 2018):

$$\rho\left(\frac{\partial u}{\partial t} + u\frac{\partial u}{\partial x} + v\frac{\partial u}{\partial y} + w\frac{\partial u}{\partial z}\right) = -\frac{\partial p}{\partial x} + \rho g_x + \mu\left(\frac{\partial^2 u}{\partial x^2} + \frac{\partial^2 u}{\partial y^2} + \frac{\partial^2 u}{\partial z^2}\right) \quad (3)$$

$$\rho\left(\frac{\partial v}{\partial t}+u\frac{\partial v}{\partial x}+v\frac{\partial v}{\partial y}+w\frac{\partial v}{\partial z}\right)=-\frac{\partial p}{\partial y}+\rho g_y+\mu\left(\frac{\partial^2 v}{\partial x^2}+\frac{\partial^2 v}{\partial y^2}+\frac{\partial^2 v}{\partial z^2}\right) \quad (4)$$

$$\rho\left(\frac{\partial w}{\partial t}+u\frac{\partial w}{\partial x}+v\frac{\partial w}{\partial y}+w\frac{\partial w}{\partial z}\right)=-\frac{\partial p}{\partial z}+\rho g_z+\mu\left(\frac{\partial^2 w}{\partial x^2}+\frac{\partial^2 w}{\partial y^2}+\frac{\partial^2 w}{\partial z^2}\right) \quad (5)$$

The conservation of momentum equation expresses Newton's second law, which states that the sum of the external forces acting on the control volume is equal to the inertial forces.
The primary external forces acting on an aircraft are viscous forces, pressure, and gravity. Lift and drag forces, in particular, arise from viscous and pressure forces.

where P is pressure (Pa), μ is viscosity (Pa.sec), g is acceleration due to gravity (m/sec^2), ρ and density (Kg/m^3), and (u, v, and w) are the velocity components on the x, y, and z directions (m/sec), respectively.

The turbulence model $k\omega{-}SST$ is more stable and dependable than the k-omega turbulence model because it employs the k-epsilon equations outside of the boundary layer region and the normal k-omega equations inside, making it more accurate close to the boundary layer region wall. With the addition of a term D_ω pertaining to the frequency dissipation of the turbulence within the α equation's bounds, the K-omega-SST turbulence model is comparable to the K-omega turbulence model (Chaoqun. L, Jiyuan. T 2018).

$$\frac{\partial(\rho\omega)}{\partial t}+\frac{\partial(\rho\omega u_j)}{\partial x_j}=\alpha\frac{\omega}{k}\tau_{ij}\frac{\partial u_i}{\partial x_j}-\gamma\rho\omega^2+\frac{\partial}{\partial x_j}\left[(\mu+\sigma_{22}\mu_t)\frac{\partial\omega}{\partial x_j}\right]+D_\omega \quad (6)$$

Whereas

$$D_\omega=2(1-F_1)\frac{\rho}{\omega\sigma_{\omega 2}}\frac{\partial k}{\partial x_j}\frac{\partial\omega}{\partial x_j} \quad (7)$$

$$F_1=tanh\left(\phi_1^4\right) \quad (8)$$

$$\phi_1=min\left[max\left(\frac{\sqrt{k}}{0.09\omega y},\frac{500\mu}{\rho y^2\omega}\right),\frac{4\rho k}{\sigma_{\omega,2}D_\omega^+ y^2}\right] \quad (9)$$

$$D_\omega^+=max\left[2\frac{\rho}{\omega\sigma_{\omega 2}}\frac{\partial k}{\partial x_j}\frac{\partial\omega}{\partial x_j},10^{-10}\right] \quad (10)$$

where τ_{ij} represents the shear stress resulting from viscosity, μ_t is vortex viscosity and μ is kinematic viscosity. The Table 2 shows the values of the constants in the previous equations (Zhao & Su 2018):

Table 2 Constant Values of K-Omega SST Turbulence Model.

$\sigma_{\omega 2}$	σ_{22}	σ_{11}	β	γ	α
1.168	1/2	1/2	9/100	3/40	5/9

2.2 Assumptions and boundary conditions

It is necessary to establish suitable boundary conditions in order to solve the previous mathematical model. These boundary conditions are displayed in Figure 2 and Table 3.

Table 3 Boundary Conditions

Velocity Inlet (Components)	Inlet
Pressure Outlet (Zero Gage Atmospheric Pressure)	Outlet
No Slip Condition	Wall Of Aircraft
Symmetry	Side Wall

The flow can be regarded as incompressible for angles of attack (0, 2, 4, 6, 8, 10, 12, and 14 degrees) because the velocity values selected for this study (20, 40, 60, and 80 m/sec) are all at Mach numbers less than 0.3, then Physical properties of air at these conditions are indicated in the Table 4.

Table 4 Physical Properties of Air

Viscosity μ(Pa.s)	$1.7894x\,10^{-5}$
density ρ(Kg/ m^3)	1.225

The study was carried out in three dimensions and in a transient state with fixed air property values.

2.3 Meshing of domain

One of the fundamental factors ensuring the validity of the numerical solution in numerical modeling is thought to be the mesh generation procedure. In order to guarantee the modeling of the viscos sublayer regime within the boundary layer, this is accomplished by testing the value of Y+ at the walls until it is extremely small (Y+<1) [39]. Figure 3 displays the mesh that was created.

Tetrahedral mesh was generated using Ansys meshing (left of Fig S1 in supplementary information) then converted to polyhedral mesh in Ansys Fluent (right of Fig S1), this ensure reducing the number of element accounts which resulted less computational cost.

A Tetrahedral mesh of five different sizes (3743532, 7742139, 9549582,13040520, and 14200000) were examine. The CL/Cd value at 80 m/Sec velocity was chosen to monitor its variation with respect to number of cells as in(see Figure S2 in supplementary information).

Since Figure 4 shows that the value of the CL/CD quantity remains constant at value of 8.96 when the number of cells reaches 13 million or more, we will use this number of cells as the cell count for numerical simulation.

2.4 Results Validation

Due to the lack of experimental results for the studied UAV and in order to verify the accuracy of the numerical results. The proposed physical model was tested with the same boundary conditions on the benchmark motion of a NACA 0012 airfoil at 1000 Reynolds number when air moves over it and starts to vibrate, as this case is similar to the vibration resulting from the movement of an airplane in the air. The Figure 5 shows the modeling of the NACA 0012 airfoil in reference (Kurtulus, 2019) which contains experimental results using the same mathematical model and boundary conditions used in the current study.

In the study (Kurtulus, 2019), the flow vibration around NACA 0012 at Reynolds number was studied and the numerical results were compared with the experimental results. The Figure 3 shows the vorticity and velocity contours for the studied wing at an angle of attack of 10 degrees and Re=1000. Figure S3 also shows the value of the instantaneous lift coefficient and its spectrum frequency at the same angle of attack. The Table 5 also shows a comparison of the experimental values with the numerical values calculated at the same angle of attack.

Table 5 Validate the Numerical Simulation

	Cl Average	Cd Average	f (Hz)
Reference [41]	0.56	0.19	4.4
Current study	0.54	0.18	4.68
Percentage error %	3.57%	5.26%	6.36%

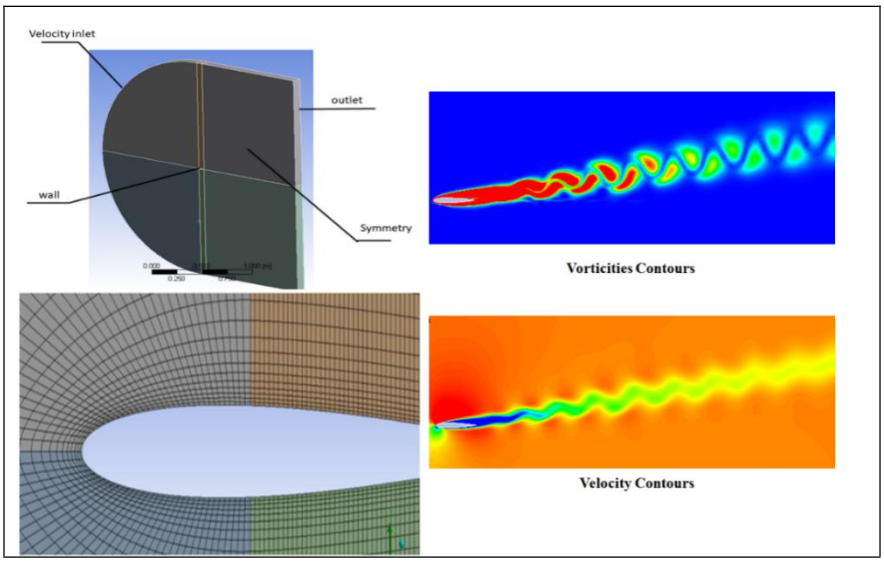

Figure 3 Benchmark of simulation validity

The average lift and drag values for different angles of attack are displayed Figure S4 (supplementary information), and a comparison of these results with experimental results (Kurtulus 2019). The Table 5 show a clear agreement between the numerically calculated and experimental values, indicating that the mathematical model and numerical modeling used in this research yield results with acceptable accuracy.

The model studied in Reference Study (Kurtulus 2019) is a 2D or planer model, meaning that the flow field does not change with the third dimension, while the Validation model is 3D and has a small thickness in order to reduce the computational cost, but it gives the same results as 2D if the area in the 2D model is set equal to the actual area studied in the 3D model. The study was done in 3D because the model studied for the aircraft is a three-dimensional model.

3. Results and Discussion

In order to solve the required mass conservation, momentum and turbulence equations in transient state, the simple algorithm was chosen as a method to velocity-pressure coupling with 0.0001 sec time step size during 2.5 sec of flow time, which requires 25000 time step number, the lift and drag coefficients were monitored and the mass conservation equation residuals were adjusted until while the rest of the equations were allowed to converge until .second order discretization were chosen for all equation.

The pressure and velocity contours around the fuselage are presented in figure S5 and S6. These contours, studied in the transient state, show the stagnation points at the front of the aircraft where the speed value is zero and the pressure is maximum, as is the case in the pressure and speed contours studied in the steady state.

In these contours, unlike the steady-state pressure and speed contours, we notice the formation of vortex separation regions behind the aircraft. These regions cannot be seen when studying flow through the fuselage in steady state.

These vortices form and separate at a specific frequency and are so small that they cannot be directly observed from the speed and pressure contours at low speeds. However, at high speeds (80 m/s), these vortices begin to appear in the speed and velocity contours, as shown in the Figure S5 and S6.

This can be explained by discussing the graphs showing the changes in the lift and drag coefficients and the lift-to-drag ratio in the Figure 4 (see figure S7/S8 for Transient Signal of Cl/Cd Coefficient).

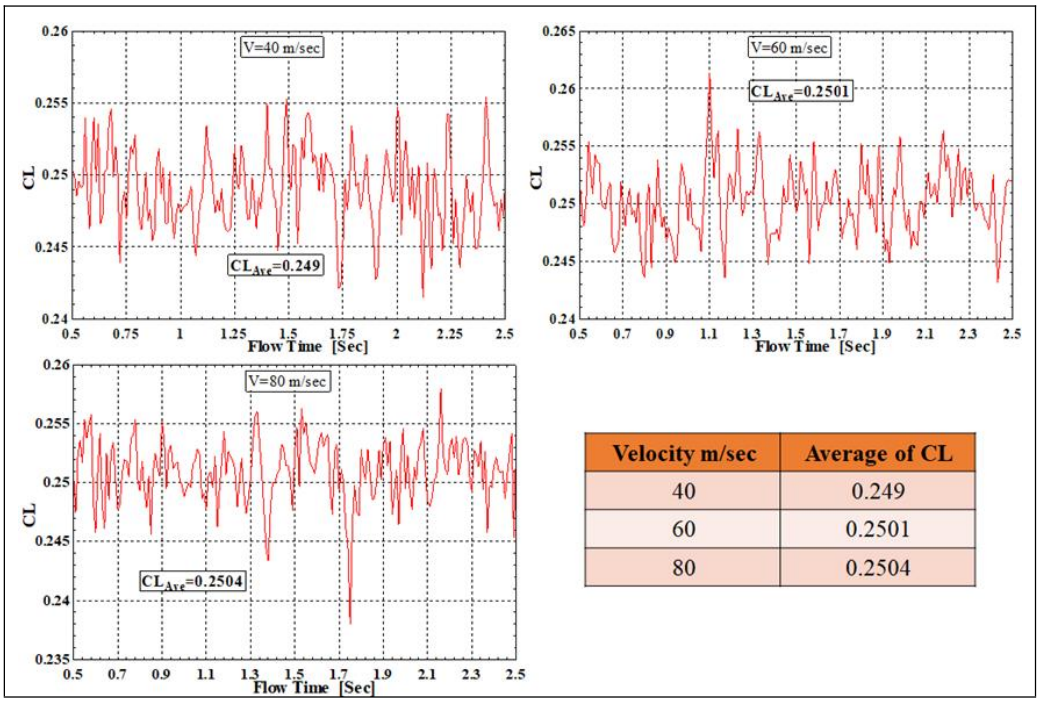

Velocity m/sec	Average of CL
40	0.249
60	0.2501
80	0.2504

Figure 4 Transient Signal of Cl Coefficient.

We note from these figures (Figure 4) the time-varying nature of the previous parameters, indicating the presence of vortices resulting from the oscillating flow behind the aircraft.

The Figure 5 also shows the average values of the drag and lift coefficients and the lift-to-drag ratio at each of the studied speeds, which are equal to the values of these coefficients when studying flow in steady state. We also note from Figure 5, as is the case in the steady state, that the value of the lift coefficient and the lift-to-drag coefficient ratio increase slightly with increasing flow velocity. the lift coefficient increases from a value of 0.249 at a speed of 40 m/sec to a value of 0.2504 at a speed of 80 m/sec, i.e., by 0.56%. The lift-to-drag coefficient ratio increases from a value of 8.711 at a speed of 40 m/sec to a value of 8.96 at a speed of 80 m/sec, i.e., by 2.85%, while the change in the value of the drag coefficient in the range of speeds studied is negligible due to the small value of the drag forces on the aircraft within the range of speeds studied.

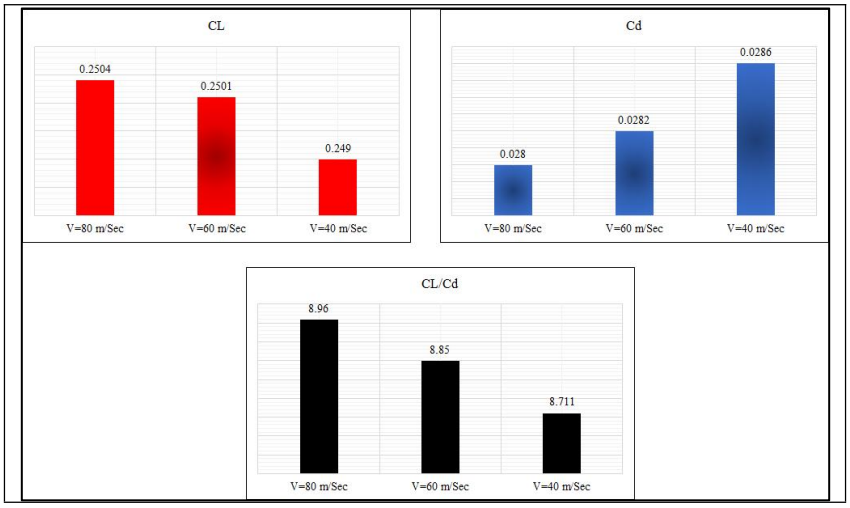

Figure 5 Average Values of Cl, Cd, CL/Cd coefficient

We notice from the figure S9 for illustration that the higher the flow velocity (aircraft speed), the greater the deviation of the instantaneous oscillation value from the average value, i.e., the higher the amplitude of the oscillation becomes. The deviation of the lift coefficient value from the average value increases from 0.65% at a speed of 40 m/sec to 1% at a speed of 80 m/sec, while the deviation of the drag coefficient value increases from 10.5% at a speed of 40 m/sec to 16.1% at a speed of 80 m/sec. The ratio of the lift coefficient to the drag coefficient increases from 31% at a speed of 40 m/sec to 36.6% at a speed of 80 m/sec. This explains the vortices seen behind the aircraft at the high speed of 80 m/sec.

To assess the severity of this fluctuations, resulting from the flow field, it is necessary to calculate the dominant flow frequencies and compare them with the natural frequency of the aircraft body to avoid these frequencies when designing the aircraft body.

By performing a fast Fourier transformer analysis of the above signals, the dominant frequency of the oscillations of both the lift coefficient and the lift-to-drag ratio can be calculated. However, we did not analyze the drag coefficient change signal because it is integrated within the lift-to-drag ratio signal.

The Figures 6 and 7 shows the fast Fourier transformer analysis of the oscillation signal of both the lift coefficient and the lift-to-drag coefficient ratio, while the Figure 17 shows the dominant frequency value at each speed.

We note from the Figure 8 that the dominant frequency of lift oscillations decreases from 11.1 Hz at 40 m/sec to 3.2 Hz at 80 m/sec, a 71.7% decrease. The frequency of lift-to-drag coefficient oscillations increases from 8.8 Hz at 40 m/sec to 17.82 Hz at 80 m/sec, a 102.5% decrease. This is due to the small changes in the drag coefficient.

The large changes in lift oscillation frequency and the low drag coefficients at high speeds within the speed range under study explain the pronounced appearance of vortices at this speed.

Future work could explore materials to reduce fouling effects on drone surfaces, similar to the solutions proposed for boiler chimneys (Kakade, 2023). Such integrations could further stabilize unsteady-state performance of drone systems in extreme environments. Further future research directions could explore specialized drone applications for food supply chains, building on the identified needs of traditional markets like Raipur's fish distribution system (Punekar, 2023). Finally, it is worth mentioning that this study should consider integrating health and environmental critiques, like the one raised by [Kumar et at] (Kumar, 2024). They discussed the exposure to drone emissions or signal interference aligns with broader concerns.

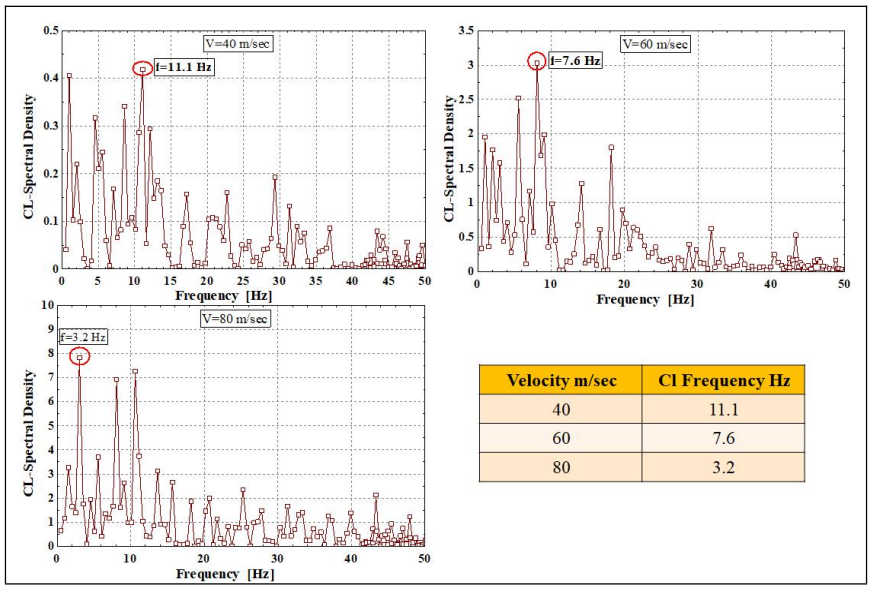

Velocity m/sec	Cl Frequency Hz
40	11.1
60	7.6
80	3.2

Figure 6 Fast Fourier transformer of CL signal.

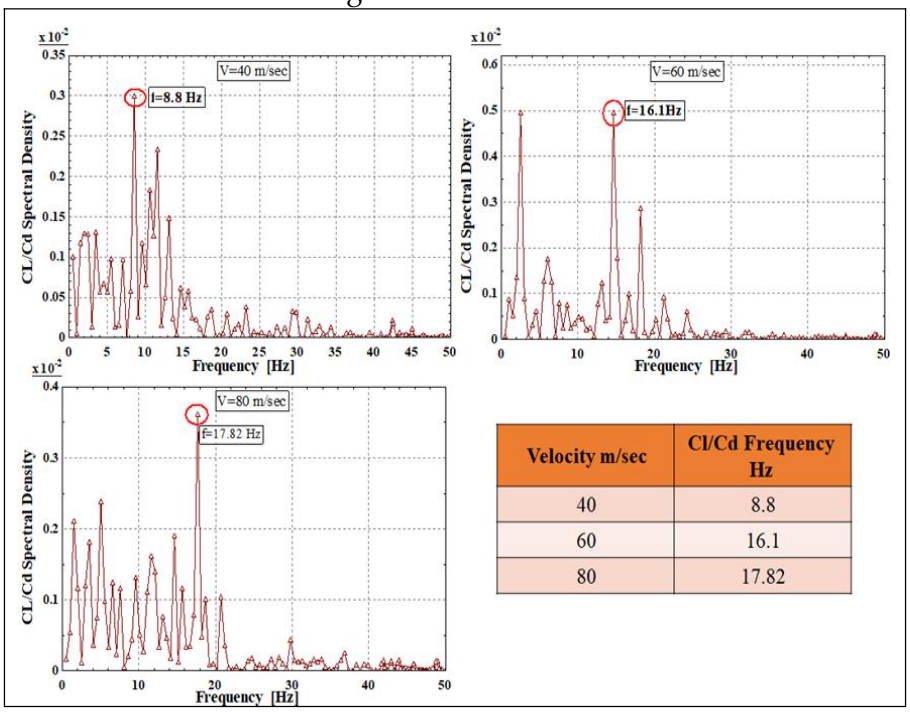

Velocity m/sec	Cl/Cd Frequency Hz
40	8.8
60	16.1
80	17.82

Figure 7 Fast Fourier transformer of CL/Cd signal

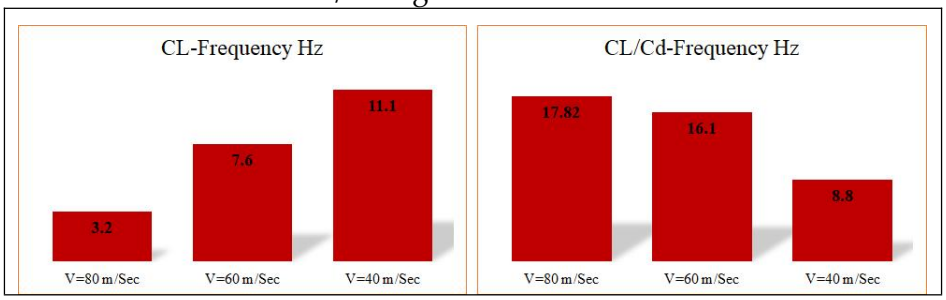

Figure 8 Values of CL and CL/CD signal dominant frequencies.

4. Conclusions

Unmanned aerial vehicle (UAV) in a transient state. The study was conducted at speeds of 40, 60, and 80 m/s at an angle of attack of 6 degrees, corresponding to the maximum value of the lift-to-drag coefficient ratio in steady state. The study was conducted numerically using Ansys Fluent. The grid-independence study was conducted, and the validity of the numerical solution was verified by comparing the results of the proposed mathematical model on NACA 0012 air foil with experimental results to confirm the validity of the mathematical model. The results of the numerical study indicate formation and decay of vortices behind the aircraft showed that the magnitude of these vortices increases with increasing aircraft speed. Additionally, lift coefficient increases by 0.56%, and the lift-to-drag ratio increases by 2.85% when the aircraft speed increases to 80 m/s. The frequency of oscillations of the lift-to-drag ratio also increases by 102.5%, while the vertical oscillation frequency corresponding to the oscillation of the lift force decreases by 71.7%. Finally, the statistical study of the standard deviation of the lift and drag coefficients and the lift-to-drag ratio from the mean value also showed an increase in these deviations with increasing aircraft speed. The standard deviation of the lift forces increases by 0.65%, the drag forces increase by 10.5%, and the lift-to-drag ratio increases by 36.6% when the aircraft speed increases from 40 m/s to 80 m/s.

Conflict of Interest

The authors declare no conflicts of interest.

Acknowledgements

I would like to express my deepest appreciation to the members of the research team, Mohammed A. Abdulwahid and Akeel MA Morad, for their invaluable contributions and collaborative spirit throughout this research paper.

Author Contributions

Sabah S. Almukhtar: Conceptualization, Methodology, Data curation, Writing- Original draft preparation. **Mohammed A. Abdulwahid:** Investigation and Supervision**. Akeel MA Morad:.** Writing- Reviewing and Editing,

Conflict of Interest

Authors declare no conflict of interest.

Supplementary Materials

Figures showing additional results of the presented research.

References

Molaa, A. A., & Abdulwahid, M. A. (2024). Numerical and experimental study of the impact on aerodynamic characteristics of the NACA0012 airfoil. *Open Engineering*, *14*(1), 20220506.

Song, J., Zhao, K., & Liu, Y. (2023). Survey on mission planning of multiple unmanned aerial vehicles. *Aerospace*, *10*(3), 208.
Zhang, S., Lin, Z., Gao, Z., Miao, S., Li, J., Zeng, L., & Pan, D. (2024). Wind tunnel experiment and numerical simulation of secondary flow systems on a supersonic wing. *Aerospace*, *11*(8), 618.
Maleki Dastjerdi, S., Gharali, K., Al-Haq, A., & Nathwani, J. (2021). Application of simultaneous symmetric and cambered airfoils in novel vertical axis wind turbines. *Applied Sciences*, *11*(17), 8011.
Majid, T., & Jo, B. W. (2021). Comparative aerodynamic performance analysis of camber morphing and conventional airfoils. *Applied Sciences*, *11*(22), 10663.
Somashekar, V. (2021). Comparative study on the prediction of aerodynamic characteristics of mini-unmanned aerial vehicle with turbulence models. *International Journal of Aviation, Aeronautics, and Aerospace*, *8*(1), 7.
Mubassira, S., Muna, F. I., & Inam, M. I. (2021). Numerical Investigation of Aerodynamic Characteristics of NACA 4312 Airfoil with Gurney Flap. *Journal of Engineering Advancements*, 2(02), 63-70.
Kumar, B. K. S., Singh, B. K. J., Niranjan, B. K., Gupta, R., 2024. Robotics is A: Boon or Disguise. *International Journal of Technology*.; 14(2), pp.139-140. doi: 10.52711/2231-3915.2024.00020
Kakade, N., Mani, A., Bhatkar C., Chaudhari, P., Roshan R., 2023. A Study on Modification of Boiler Chimney against Fouling to Enhance: The Efficiency of Boiler. *International Journal of Technology*, 13(1), pp.22-24. doi: 10.52711/2231-3915.2023.00003
Patel, A. B., Gol, A. M., Vyas, A. J., Patel, A, I., Dudhrejiya, A. V., Chotaliya, U. J, 2023. A brief review on PET - Polyethylene Terephthalate Containers. *International Journal of Technology*, 13(1), pp.50-56. doi: 10.52711/2231-3915.2023.00006
Sharma, P., Kumari, A., Shivali, Sharma V. 2024. Impact of Food and Health in 21st Century Era: A Global Economic Crises. *International Journal of Technology*. 14(2), pp111-1114. doi: 10.52711/2231-3915.2024.00016
Punekar, S., Sahu, S., Kumar A., Agrawal, A. 2023. Study of Fish Markets and their Pattern of Raipur City. *International Journal of Technology*, 13(1), p.35-40. doi: 10.52711/2231-3915.2023.00004
Amsallem, D., Cortial, J. & Farhat, C., 2010. Towards real-time computational-fluid-dynamics-based aeroelastic computations using a database of reduced-order information. *AIAA journal*, 48(9), pp.2029–2037. doi: 10.2514/1.j050233.
Andersson, B. et al., 2012. *Computational fluid dynamics for engineers*, Cambridge university press. doi: 10.1017/cbo9781139093590.
Bernitsas, M.M. et al., 2008. VIVACE (Vortex Induced Vibration Aquatic Clean Energy): A new concept in generation of clean and renewable energy from fluid flow. *Journal of Offshore Mechanics and Arctic Engineering 130*.
Bibo, A. & Daqaq, M.F., 2015. An analytical framework for the design and comparative analysis of galloping energy harvesters under quasi-steady aerodynamics. *Smart Materials and Structures*, 24(9), p.94006. doi: 10.1088/0964-1726/24/9/094006.
Boelens, O.J., 2012. CFD analysis of the flow around the X-31 aircraft at high angle of attack. *Aerospace Science and Technology*, 20(1), pp.38–51. doi: 10.1016/j.ast.2012.03.003.
Buchholz, J.H.J. & Smits, A.J., 2008. The wake structure and thrust performance of a rigid low-aspect-ratio pitching panel. *Journal of fluid mechanics*, 603, pp.331–365. doi: 10.1017/s0022112008000906.
Chaoqun. L, Jiyuan. T, G.H., 2018. *Computational fluid dynamics: a practical approach*, Elsevier Inc.
Dickes, E., Ralston, J. & Lawson, K., 2000. Application of large-angle data for flight simulation. In *Modeling and Simulation Technologies Conference*. p. 4584. doi: doi.org/10.2514/6.2000-4584.
Dowell, E.H., Hall, K.C. & Romanowski, M.C., 1997. Eigenmode analysis in unsteady aerodynamics: Reduced order models. doi: 10.1115/1.3101718.
Fischenberg, D. & Jategaonkar, R. V, 1998. Identification of aircraft stall behavior from flight test data. In *RTO SCI Symposium on System Identification for Integrated Aircraft Development and Flight Testing*. NATO Neuilly-Sur-Seine Cedex, France.
Fransos, D. & Bruno, L., 2006. Determination of the aeroelastic transfer functions for streamlined bodies by means of a Navier–Stokes solver. *Mathematical and computer modelling*, 43(5–6), pp.506–529. doi: 10.1016/j.mcm.2005.10.002.

Gold, P. & Karpel, M., 2008. Reduced-size aeroservoelastic modeling and limit-cycle-oscillation simulations with structurally nonlinear actuators. *Journal of Aircraft*, 45(2), pp.471–477. doi: 10.2514/1.28933.

Green, M.A. & Smits, A.J., 2008. Effects of three-dimensionality on thrust production by a pitching panel. *Journal of fluid mechanics*, 615, pp.211–220. doi: 10.1017/s0022112008003583.

Green, W.E. & Oh, P.Y., 2009. A hybrid MAV for ingress and egress of urban environments. *IEEE Transactions on Robotics*, 25(2), pp.253–263. doi: 10.1109/tro.2009.2014501.

Green, W.E. & Oh, P.Y., 2005. A MAV that flies like an airplane and hovers like a helicopter. In *Proceedings, 2005 IEEE/ASME International Conference on Advanced Intelligent Mechatronics.* IEEE, pp. 693–698. doi: 10.1109/aim.2005.1511063.

Johnson, B. & Lind, R., 2009. High angle-of-attack flight dynamics of small UAVs. In *47th AIAA Aerospace Sciences Meeting Including The New Horizons Forum and Aerospace Exposition*. p. 61. doi: 10.2514/6.2009-61.

Kaplan, S.M., Altman, A. & Ol, M., 2007. Wake vorticity measurements for low aspect ratio wings at low Reynolds number. *Journal of Aircraft*, 44(1), pp.241–251. doi: 10.2514/1.23096.

Klein, V. & Morelli, E., 2006. *Aircraft System Identification: Theory And Practice*, doi: 10.2514/4.861505.

Kubo, D., 2006. Study on design and transitional flight of tail-sitting VTOL UAV. In *Proceedings of 25th Congress of ICAS*.

Kurtulus, D.F., 2019. Unsteady aerodynamics of a pitching NACA 0012 airfoil at low Reynolds number. *International Journal of Micro Air Vehicles*, 11, p.1756829319890609. doi: 10.1177/1756829319890609.

Leishman, G.J., 2006. *Principles of helicopter aerodynamics with CD extra*, Cambridge university press.

Leishman, J.G., Bhagwat, M.J. & Ananthan, S., 2002. Free-vortex wake predictions of the vortex ring state for single-rotor and multi-rotor configurations. In *AHS International, 58 th Annual Forum Proceedings-*. pp. 642–671.

Mor, M. & Livne, E., 2005. Minimum-state unsteady aerodynamics for aeroservoelastic configuration shape optimization of flight vehicles. *AIAA journal*, 43(11), pp.2299–2308. doi: 10.2514/1.10005.

Murman, S.M., 2007. Reduced-frequency approach for calculating dynamic derivatives. *AIAA journal*, 45(6), pp.1161–1168. doi: 10.2514/6.2005-840.

Ol, M. et al., 2005. Comparison of laminar separation bubble measurements on a low Reynolds number airfoil in three facilities. In *35th AIAA fluid dynamics conference and exhibit*. p. 5149. doi: 10.2514/6.2005-5149.

Pelletier, A. & Mueller, T.J., 2000. Low Reynolds number aerodynamics of low-aspect-ratio, thin/flat/cambered-plate wings. *Journal of aircraft*, 37(5), pp.825–832. doi: 10.2514/2.2676.

Ronch, A. Da et al., 2012. Evaluation of dynamic derivatives using computational fluid dynamics. *AIAA journal*, 50(2), pp.470–484. doi: 10.2514/1.j051304.

Roy, S., Moreau, A. & Grosbois, M., 2007. Modeling and Simulation of a Forward-Swept Wing, Vertical Takeoff or Landing & Thrust Vectored Remotely Piloted Vehicle. In *Proc. Canadian Aeronautics and Space Institute Annual General Meeting on Aircraft Design and Development Symposium*.

Schlichting, H. & Truckenbrodt, E., 1979. *Aerodynamics of the Airplane*, McGraw-Hill. Available at: https://books.google.iq/books?id=A80eAQAAIAAJ.

Selig, M., 2010. Modeling full-envelope aerodynamics of small UAVs in realtime. In *AIAA Atmospheric Flight Mechanics Conference*. p. 7635. doi: 10.2514/6.2010-7635.

Silva, W.A. & Bartels, R.E., 2004. Development of reduced-order models for aeroelastic analysis and flutter prediction using the CFL3Dv6. 0 code. *Journal of Fluids and Structures*, 19(6), pp.729–745. doi: 10.1016/j.jfluidstructs.2004.03.004.

Singh, R. & Baeder, J.D., 1997. Direct calculation of three-dimensional indicial lift response using computational fluid dynamics. *Journal of Aircraft*, 34(4), pp.465–471. doi: 10.2514/2.2214.

Sitaraman, J. & Baeder, J.D., 2004. Computational-fluid-dynamics-based enhanced indicial aerodynamic models. *Journal of aircraft*, 41(4), pp.798–810. doi: doi.org/10.2514/1.12419.

Taira, K. & Colonius, T., 2009. Effect of tip vortices in low-Reynolds-number poststall flow control. *AIAA journal*, 47(3), pp.749–756. doi: doi.org/10.2514/1.40615.

Taira, K. & Colonius, T.I.M., 2009. Three-dimensional flows around low-aspect-ratio flat-plate wings at low Reynolds numbers. *Journal of Fluid Mechanics*, 623, pp.187–207. doi: doi.org/10.1017/s0022112008005314.

Theodorsen, T., 1979. GENERAL THEORY OF AERODYNAMIC INSTABILITY AND THE MECHANISM OF. *Classical Aerodynamic Theory*, 1050, p.291.

Wagner, H., 2006. Uber die Entstehung des Dynamischen Auftriebs von Tragugeln. *ZAMM - Journal of Applied Mathematics and Mechanics / Zeitschrift für Angewandte Mathematik und Mechanik*, 5, pp.17–35. doi: 10.1002/zamm.19250050103.

Williams, D. et al., 2008. Control of flow structure on a semi-circular planform wing. In *46th AIAA Aerospace Sciences Meeting and Exhibit*. p. 597. doi: 10.2514/6.2008-597.

Zhao, Y. & Su, X., 2018. *Computational fluid-structure interaction: Methods, models, and applications*, Academic Press.

Blevins, R. D. (1977). Flow-induced vibration. New York.